**Mingyao Li**
School of Mechanics and Civil Engineering,
China University of Mining and Technology,
Beijing 100083, China;
State Key Laboratory of Nonlinear Mechanics,
Institute of Mechanics,
Chinese Academy of Sciences,
Beijing 100190, China
e-mail: mingyao.li@cumtb.edu.cn

**Xin Chen**
School of Mechanics and Civil Engineering,
China University of Mining and Technology,
Beijing 100083, China
e-mail: chx@cumtb.edu.cn

**Dong Zhou**[1]
State Key Laboratory of Nonlinear Mechanics,
Institute of Mechanics,
Chinese Academy of Sciences,
Beijing 100190, China
e-mail: zhoudong@imech.ac.cn

**Yewang Su**[1]
State Key Laboratory of Nonlinear Mechanics,
Institute of Mechanics,
Chinese Academy of Sciences,
Beijing 100190, China;
School of Engineering Science,
University of Chinese Academy of Sciences,
Beijing 100049, China;
Department of Engineering Mechanics,
State Key Laboratory of Structural
Analysis for Industrial Equipment,
Dalian University of Technology,
Dalian 116024, China
e-mail: yewangsu@imech.ac.cn

# A Spectral Microplane Model for the Anisotropic Damage Behavior of Shales

*The development of constitutive models for shales has been a challenge for decades due to the difficulty of characterizing the strongly anisotropic macroscopic behavior related to the inherent mesostructure and damage mechanisms. In this paper, a spectral microplane damage model is developed for the anisotropic damage behavior of shales. The modeling challenge of the anisotropic elasticity in the microplane model is theoretically overcome by the spectral decomposition theory without limitation on the degree of the anisotropy compared with other microplane models. The stiffness tensor of anisotropic shales is effectively decomposed into four different eigenmodes with the activation of certain groups of microplanes corresponding to the specific orientation of the applied stresses. The inherent and the induced anisotropic behavior is thus characterized by proposing suitable microplane relations on certain eigenmodes directly reflecting the initial mesostructure and the failure mechanisms. For the challenge of the postpeak softening behavior, two-scalar damage variables are introduced to characterize the tensile and the shear damage related to the opening and the closure of microcracks under different stress conditions. Comparison between numerical simulation and experimental data shows that the proposed model provides satisfactory predictions for both weakly and highly anisotropic shales including prepeak nonlinear behavior, failure strengths, and postpeak softening under different confining pressures and different bedding plane orientations.* [DOI: 10.1115/1.4047005]

*Keywords: constitutive models, anisotropy, damage, spectral decomposition, shales, constitutive modeling of materials, failure criteria, mechanical properties of materials, plasticity*

## 1 Introduction

Despite a number of research efforts have been devoted to study the mechanical behavior of rocks, the thorough understanding of the anisotropic deformation properties and failure mechanisms is still a major challenge in many geotechnical applications, such as the hydraulic fracturing, the geotechnical excavations, and the radioactive waste disposal [1,2]. Most recently, the increasing attention on shale gas has appealed many research interests to deeply investigate the anisotropic behavior of shales [3–5]. Many laboratory investigations have been conducted to study the anisotropic deformation behavior and failure modes for shales [6–10]. Most experimental results exhibit a strong inherent and induced anisotropy with a directional dependence of deformation characteristics. The strengths and the failure modes vary with the angle between the loading direction and the bedding planes. It is also indicated that the intrinsic and induced anisotropic behavior is strongly characterized by the mesostructure, such as the existence of bedding planes. Essentially, the macroscopic inelastic behavior of anisotropic shales is primarily characterized by the mesoscopic mechanisms including the plastic deformation, the microcracks-induced damage, the splitting, and the shear slipping regarding the weak bedding planes.

A large number of constitutive models have also been proposed to describe the plastic deformation and the failure criteria for anisotropic rocks. A comprehensive review on this subject has been conducted to investigate different methods, such as the mathematical approach, the empirical approach, and the discontinuous weakness plane-based approach [11]. In general, the mathematical models are theoretically rigorous based on the tensorial formulations but too complex to solve the practical engineering problems [12]. The empirical models are phenomenal in nature, thereby lacking clear physical interpretations and not capable of considering the effects of the mesostructure [13]. The discontinuous weakness plane models are generally suitable for anisotropic rocks due to the consideration of the physical mechanism of the failure process, but the limitation is the complicated numerical implementation [14,15]. Recently, microscopic constitutive models have been developed based on the microstructure of anisotropic rocks [16,17]. This approach is mathematically rigorous with simple formulations and thus successfully applied to define failure criterion of anisotropic rocks. However, it is still a major challenge for these models to fully consider the anisotropic rocks in particular the highly anisotropic ones such as shales. The main problem is the complex tensorial formulated description of oriented deformation including the elastic, the plastic, and the damage behavior induced by the splitting and the shear slipping regarding the weak bedding layers. Therefore, the highly intrinsic anisotropic properties coupled with the oriented plastic and the damage behavior induced by the mesostructure often demand very complex form of constitutive laws.

[1]Corresponding authors.

Contributed by the Applied Mechanics Division of ASME for publication in the Journal of Applied Mechanics. Manuscript received February 24, 2020; final manuscript received April 12, 2020; published online May 14, 2020. Assoc. Editor: A. Amine Benzerga.

  

Alternatively, the oriented behavior can be straightforwardly characterized by the microplane model based on the concept of vectoral constitutive relations on the tangent planes of a unit sphere surrounding every material point [18]. This concept degrades the traditional constitutive tensor model as the simple vectoral formulations which significantly reduce the complexity of the problem. The introduction of the concept "microplane" fundamentally enables the constitutive model to be established on many generic planes with different orientations to represent the certain mechanical behavior of each direction [19]. Based on these advantages, the microplane model was progressively established as a fully developed theory for the damage behavior of the quasi-brittle materials [20]. In the last few decades, it has been widely applied to concretes as the progressive softening damage constitutive model and also successfully applied in other complex materials such as rocks, fiber composites, foams, and some weak anisotropic materials, e.g., clays, but only limited to weak anisotropic materials [21,22]. The challenge for pronounced anisotropic materials is still open for discussion. Most recently, the attention was called on a similar work for shales and other anisotropic rocks by a spherocylindrical microplane constitutive model [23]. The new model is mathematically elegant and verified for the high degree of anisotropy. However, for strongly anisotropic shales, e.g., the elastic in-plane to out-plane moduli ratio is higher than 3.75, it is still impossible to mathematically guarantee the consistent relationship between the microplane elastic vectors and the macroscopic elastic tensor. Meantime, the spectral microplane model has been rigorously proven as the only version of the microplane model to characterize the anisotropy without limitation [24]. The spectral microplane model theoretically solves the rigorous correspondence between the microplane vector and the macroscopic tensor without limitation on the degree of anisotropy compared with other microplane models.

For this purpose, we develop a spectral microplane damage model for the anisotropic damage behavior of shales without limitation on the degree of the anisotropy. The directional properties related to the inherent mesostructure and damage mechanisms are described by proposing appropriate microplane laws on the eigenmodes decomposed from the stiffness tensor of anisotropic shales. In order to describe the material softening behavior due to the oriented distribution of induced microcracks, two-scalar damage variables are introduced to characterize the strong dissymmetry damage mechanism under the tensile and the compressive conditions. The proposed model is applied to a weakly anisotropic shale, and the comparisons between numerical results and experimental data show very satisfactory predictions for the prepeak nonlinear behavior, the failure strength, and the postpeak softening under different confining pressures and different bedding plane orientations. Further validation of the predictive ability for highly anisotropic shales is performed, and the numerical results are also generally agreed with the experimental data.

## 2 The Spectral Microplane Framework and Application to Shales

**2.1 The Formulation of the Spectral Microplane Model.** The formulation of the microplane model based on the spectral decomposition theory is recalled in the following [24]. The elastic stress–strain relation of anisotropic shales can be expressed in the matrix notation as

$$(\boldsymbol{\sigma}) = [\boldsymbol{C}](\boldsymbol{\varepsilon}) \tag{1}$$

where $(\boldsymbol{\sigma})$ and $(\boldsymbol{\varepsilon})$ are the stress and the strain matrix in the form of six-dimensional vector, $[\boldsymbol{C}]$ is the $6\times6$ dimensional elastic stiffness matrix. According to the spectral decomposition theorem, it can be decomposed as

$$[\boldsymbol{C}] = \sum\nolimits_I \lambda_I [\boldsymbol{C}_I] \tag{2}$$

where $\lambda_I$ is the eigenvalue and $[\boldsymbol{C}_I]$ is the eigenmatrix corresponding to each other with the subscript $I$ (Appendix C).

In order to compare with the traditional microplane model, the procedure of the spectral microplane model is outlined as illustrated in Fig. 1.

(1) Combining the spectral decomposition theorem and the kinematic constraint, the macroscopic strain $(\boldsymbol{\varepsilon})$ can be projected to be the microplane eigenstrain $(\boldsymbol{\varepsilon}_{PI})$

$$(\boldsymbol{\varepsilon}_{PI}) = [P_I](\boldsymbol{\varepsilon}) \tag{3}$$

where $[P_I] = [P][\boldsymbol{C}_I]$, $[P]$ is the project matrix (Appendix A).

(2) The microplane eigenstress $(\boldsymbol{\sigma}_{PI})$ is obtained by the spectral microplane constitutive laws

$$(\boldsymbol{\sigma}_{PI}) = f(\boldsymbol{\varepsilon}_{PI}) \tag{4}$$

(3) The macroscopic stress $(\boldsymbol{\sigma})$ is calculated by the principle of virtual work

$$(\boldsymbol{\sigma}) = \frac{3}{2\pi}\int_\Omega [P]^T \sum\nolimits_I (\boldsymbol{\sigma}_{PI}) d\Omega \tag{5}$$

where $\Omega$ is the surface of a unit hemisphere and $[P]^T$ is the transpose of the projection matrix.

**2.2 Application to Transversely Isotropic Shales.** The anisotropic shales are known as typical transversely isotropic materials and the anisotropic features are strongly related to the inherent bedding layers as shown in Fig. 2(*a*). Thus, the elastic tensor of shales is a function of the direction of the bedding planes relating to the orientation of the coordinates. As shown in Fig. 2(*b*), the angle between the bedding layers ($S_1 - O - S_2$ local coordinate system) and the loading direction (the uniform arrows along $z$-axis in the $z-o-y$ global coordinate system) is $\alpha$, where $\alpha = 0$ deg indicates that the loading direction is parallel to the bedding planes, and $\alpha = 90$ deg perpendicular to the bedding layers.

Thanks to the transformation of the stress and strain components (Appendix B), the material matrix in the microplane model remains unchanged, and the corresponding eigenvalues and featured matrices remain the same. After the macrostress is calculated, an inverse transformation can be performed to obtain the final macrostress.

**2.3 Analysis of Microplane Eigenstrain Modes and Physical Interpretation.** The transversely isotropic shales possess a rotation axis ($z$ axis) with five independent elastic parameters as shown in Fig. 2(*a*). The elastic parameters of the anisotropic direction ($z$ axis) are denoted as $E_\perp$, $\nu_\perp$ and the ones of the isotropic direction ($x/y$ direction) $E_{/\!/}$, $\nu_{/\!/}$, $G_{/\!/}$. The corresponding elastic compliance matrix $[\boldsymbol{S}]$ is expressed as

$$[\boldsymbol{S}] = \begin{bmatrix} \frac{1}{E_{/\!/}} & -\frac{\nu_{/\!/}}{E_{/\!/}} & -\frac{\nu_\perp}{E_{/\!/}} & 0 & 0 & 0 \\ -\frac{\nu_{/\!/}}{E_{/\!/}} & \frac{1}{E_{/\!/}} & -\frac{\nu_\perp}{E_{/\!/}} & 0 & 0 & 0 \\ -\frac{\nu_\perp}{E_{/\!/}} & -\frac{\nu_\perp}{E_{/\!/}} & \frac{1}{E_\perp} & 0 & 0 & 0 \\ 0 & 0 & 0 & \frac{1}{2G_{/\!/}} & 0 & 0 \\ 0 & 0 & 0 & 0 & \frac{1}{2G_{/\!/}} & 0 \\ 0 & 0 & 0 & 0 & 0 & \frac{1+\nu_{/\!/}}{E_{/\!/}} \end{bmatrix} \tag{6}$$

The microplane eigenstrain vector $(\boldsymbol{\varepsilon}_{PI}) = (\varepsilon_{NI}, \varepsilon_{MI}, \varepsilon_{LI})^T$ can be thus calculated according to Eq. (A7) and the analytical formulae of strain modes components are reported in the Table 1. The angle $\theta$ and $\varphi$ are the microplane spherical angles as illustrated in Fig. 2(*c*) and $\alpha_1$, $\alpha_2$, $\alpha_3$ are the macroscopic strain functions. It is noted that the microplane eigenstrain components $\varepsilon_{NI}$, $\varepsilon_{MI}$, $\varepsilon_{LI}$

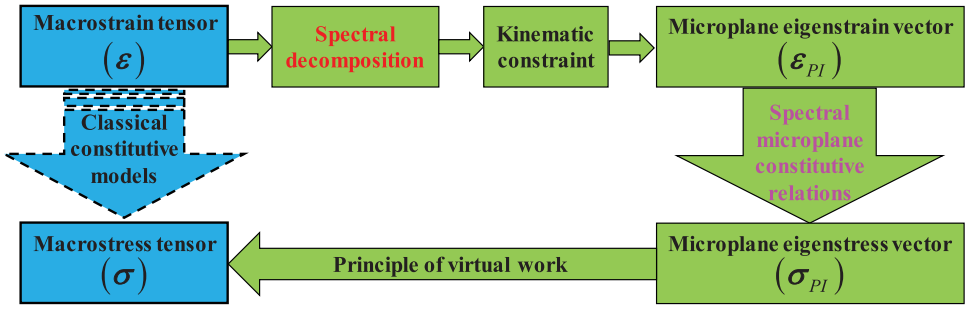


**Fig. 1 Flowchart of the calculation of the spectral microplane model**

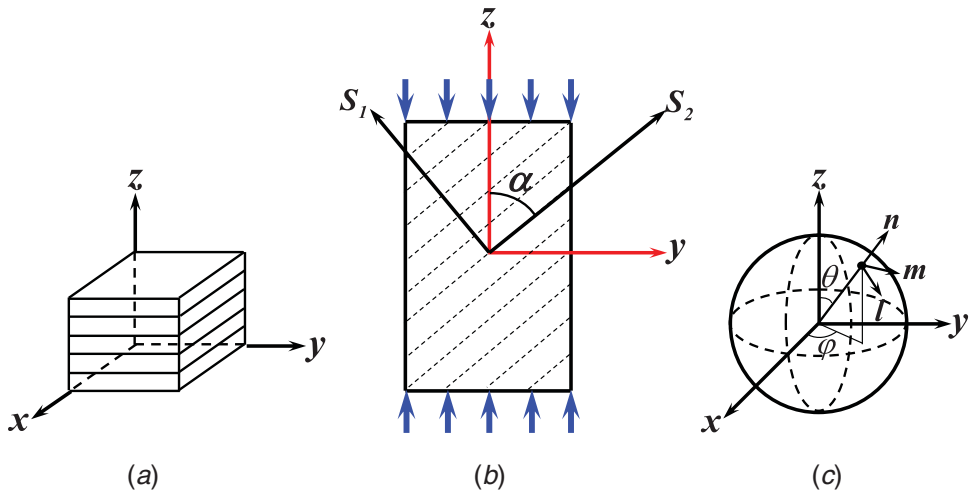


**Fig. 2 (*a*) Illustration of the structure of transversely isotropic materials, (*b*) definition of the angle $\alpha$, and (*c*) spherical coordinates**

depend on the parameters of $\alpha_1$, $\alpha_2$, $\alpha_3$, $\varepsilon_4$, $\varepsilon_5$, $\varepsilon_6$, $\theta$, $\varphi$, and $\omega$. Namely, the microplane eigenstrain modes are strongly affected by the macroscopic strain. Therefore, three typical loading directions on transversely isotropic shales are analyzed with physical interpretation for the distribution of normal strain components.

As the macroscopic uniaxial strain is applied in the anisotropic direction (Fig. 3(*a*)), it is found that only normal components of the modes II and III are nonzero but the modes I and IV are exactly zero. It means that the response in anisotropic direction depends only on the modes II and III but independent from the modes I and IV. As can be noted from Figs. 3(*b*) and 3(*c*), the distribution of the two active normal strain components on the microplane sphere is illustrated for a weakly anisotropic shale ($\omega = 0.5365$) and a highly anisotropic shale ($\omega = 0.218$). It is indicated that the normal strain of mode II is near-uniformly distributed for the weakly anisotropic shale. The magnitude of the anisotropic distribution for the highly anisotropic shale is negligible compared with the one of the mode III. On the contrary, the distribution of the mode III is strongly anisotropic representing that the microplanes are mainly activated along the loading direction matching exactly with the structure of the bedding planes. This analysis reveals that the response of shales subjected to the loading along the anisotropic direction strongly depends on the behavior of the bedding planes and can be dominated by mode III.

As the macroscopic uniaxial strain is applied in the transverse direction (Fig. 5(*a*)), the normal strains of modes I, II, and III are nonzero which means that these three modes codetermine the property in the transverse direction. The distribution of the three active normal strains on the microplane sphere is shown in Figs. 4(*b*)–4(*d*). For the highly anisotropic shale, the normal strain of modes I and III are negligible compared with mode II. The corresponding microplanes are mainly activated in transverse direction which is completely opposite to the case of the anisotropic loading direction. Thus, the response of the highly anisotropic shale subjected to the loading in the transverse direction strongly depends on the matrix of the shale and can be mainly controlled by mode II. For the weak anisotropic shale, the distribution of modes I and III is slightly directional in 3-axis and 2-axis, respectively, but mode II acts volumetrically. It reveals that the properties of the matrix are codetermined by all three active modes.

As expected from the formulae of the strain components in Table 1, the normal strain of mode IV is only activated for the

**Table 1 Microplane eigenstrains: normal and tangential components [24]**

| Mode | Normal component $\varepsilon_N$ | Tangential component $\varepsilon_M$ | Tangential component $\varepsilon_L$ |
|---|---|---|---|
| I | $\sin^2\theta[\alpha_1(\cos^2\varphi - \sin^2\varphi) + 2\varepsilon_6 \sin\varphi\cos\varphi]$ | $\sin\theta\cos\theta[\alpha_1(\cos^2\varphi - \sin^2\varphi) + 2\varepsilon_4 \sin\varphi\cos\varphi]$ | $\sin\theta[-2\alpha_1 \sin\varphi\cos\varphi + \varepsilon_6(\cos^2\varphi - \sin^2\varphi)]$ |
| II | $\alpha_3(\cos\omega \sin^2\theta/\sqrt{2} + \sin\omega\cos^2\theta)$ | $\alpha_3 \sin\theta\cos\theta(\cos\omega/\sqrt{2} - \sin\omega)$ | 0 |
| III | $\alpha_2(-\sin\omega \sin^2\theta/\sqrt{2} + \cos\omega\cos^2\theta)$ | $\alpha_2 \sin\theta\cos\theta(-\sin\omega/\sqrt{2} - \cos\omega)$ | 0 |
| IV | $2\sin\theta\cos\theta(\varepsilon_4 \sin\varphi + \varepsilon_5\cos\varphi)$ | $(\cos^2\theta - \sin^2\theta)(\varepsilon_4 \sin\varphi + \varepsilon_5\cos\varphi)$ | $\cos\theta(\varepsilon_4\cos\varphi - \varepsilon_5 \sin\varphi)$ |

Notes: $\alpha_1 = (\varepsilon_1 - \varepsilon_2)/2$, $\alpha_2 = -\sin\omega(\varepsilon_1 + \varepsilon_2)/\sqrt{2} + \varepsilon_3\cos\omega$, $\alpha_3 = \cos\omega(\varepsilon_1 + \varepsilon_2)/\sqrt{2} + \varepsilon_3 \sin\omega$

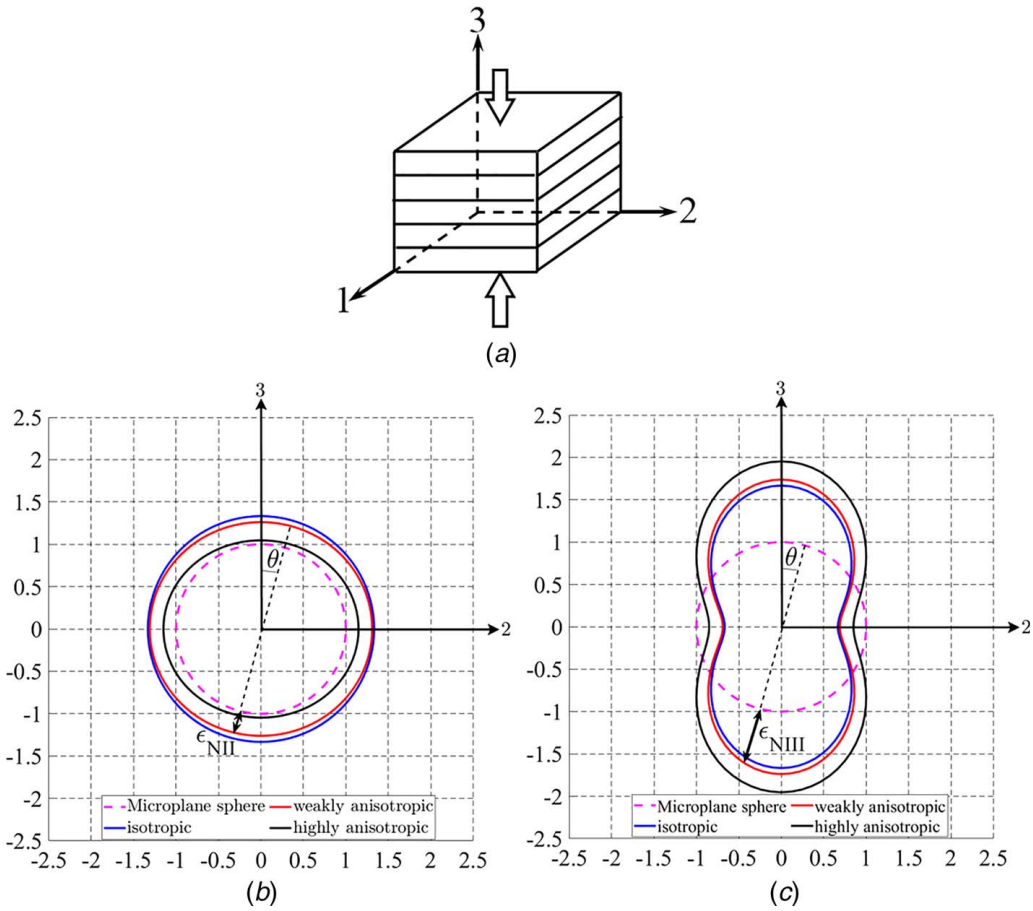


**Fig. 3 Distribution of the normal strain components for the macroscopic strain in the anisotropic direction: (*a*) illustration of the structure frame and the lording direction, (*b*) mode II, and (c) mode III**

shear macroscopic strain (Fig. 5(*a*)) which mainly acts on the microplanes in the direction $\theta = 45$ deg as illustrated in Fig. 5(*b*). It reveals that the shear behavior is highly dominated by the bedding planes such as shear slip mechanism.

The above analysis shows that the anisotropic properties of the transversely isotropic shales are strongly related to its microstructures. The anisotropic behavior is dominated by the bedding planes, while the transverse properties are mainly related to the matrix. Owing to the stiffness decomposition, the anisotropic properties can be effectively decomposed into different eigenstrain modes with specific activation of microplanes for description of the directional behavior.

## 3 The Formulation of the Damage Constitutive Model

Based on the above analysis, the mechanical behavior of shales can be characterized by defining constitutive relations on the decomposed eigenmodes instead of directly on microplanes. In Sec. 3, emphasis is on the definition of microplane constitutive laws by considering the mesostructure and failure mechanism of transversely isotropic shales.

According to the spectral microplane framework, in the elastic phase the eigenstress and eigenstrain satisfy the proportional relationship, and the normal eigenstress $\sigma_{NI}$ and the two shear eigenstresses $\sigma_{MI}$, $\sigma_{LI}$ are corresponding to the eigenmodes of each microplane

$$\sigma_{NI} = \lambda_I \varepsilon_{NI}, \quad \sigma_{MI} = \lambda_I \varepsilon_{MI}, \quad \sigma_{LI} = \lambda_I \varepsilon_{LI} \tag{7}$$

where $\varepsilon_{NI}$, $\varepsilon_{MI}$, $\varepsilon_{LI}$ represent the normal eigenstrain and the two shear eigenstrains on the $I$th eigenmode, and $\lambda_I$ the $I$th eigenvalues. The total eigenstress must satisfy the specific stress–strain boundaries

$$\sigma_I^{b-}(\varepsilon_I, \varepsilon_{II}, \theta, \ldots h) \le \sigma_I \le \sigma_I^{b+}(\varepsilon_I, \varepsilon_{II}, \theta, \ldots h) \tag{8}$$

where $\sigma_I^{b+}$ and $\sigma_I^{b-}$ are the tensile and the compressive boundaries in function of the eigenstrains $\varepsilon_I$, $\varepsilon_{II}$…, the spherical angle $\theta$, and the internal variables $h$. These two stress–strain boundaries are defined to simulate the inherent and the induced anisotropic characteristics.

**3.1 The Modeling of the Inelastic Behavior.** The inelastic response of shales can be described by the stress–strain boundaries on the microplane which are equivalent to the yield function of the traditional plasticity theory [25]. The key advantage of this concept is that different independent boundaries for different stress components can be defined on the same microplane, namely, stress components on the same microplane are independent of each other. It is completely different from the tensorial constitutive relations and quite convenient to characterize the anisotropic behavior from the microscopic level. The aim of this section is to define the inelastic behavior of the transversely isotropic shales according to the main physical phenomena of the microscopic level, such as the effects of the microstructures and failure mechanism related to the bedding planes.

It is known that the mechanical behavior of shales strongly depends on the loading path. For example, the dissymmetry between the responses under tensile and compressive stress is related to the open and closure of microcracks while the shear failure essentially associated with the frictional sliding along microcracks surfaces. For this purpose, three stress–strain boundaries are proposed similar to the traditional microplane model, i.e., the normal tensile stress boundary, the normal compressive stress boundary, and the shear stress boundary.

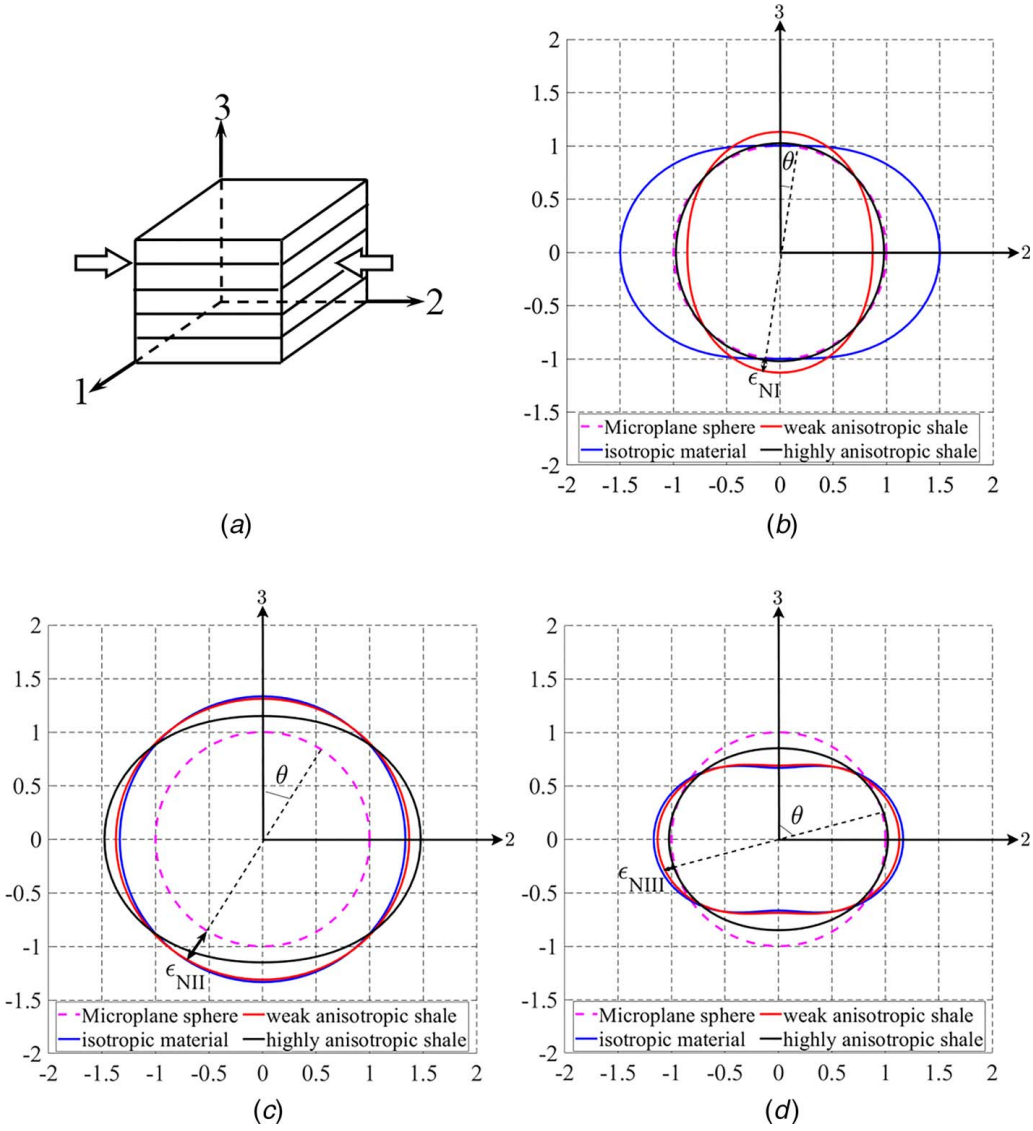


**Fig. 4 Distribution of the normal strain components for the uniaxial macroscopic strain in the transverse direction: (*a*) illustration of the structure frame and the lording direction, (*b*) mode I, (c) mode II, and (*d*) mode III**

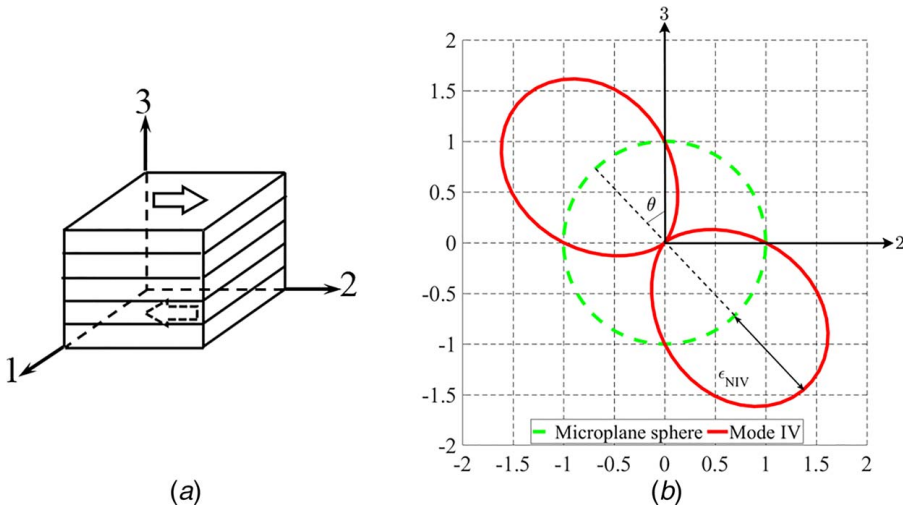


**Fig. 5 Distribution of the normal strain components for the shear macroscopic strain in the transverse direction: (*a*) illustration of the structure frame and the lording direction and (*b*) mode IV**

(1) Normal tensile stress boundary

The normal tensile stress boundary is proposed to describe the tensile failure and the microcracks-induced damage, in particular the opening and propagation mechanism under tensile stress [26]. In other words, the normal tensile stress boundary is used to limit the tensile stress $\sigma_N^{b+}$. It is known that the tensile strength is constant for isotropic materials but varies with the orientation of the bedding layers for anisotropic shales, namely, the strength is a function of the spherical angle $\theta$ (Fig. 2(*b*)). Thus, the normal tensile stress boundary equation $\sigma_N^{b+}$ can be formulated as

$$\sigma_N^{b+} = T_0\alpha(\theta) \tag{9}$$

where $T_0$ is the reference tensile strength, $\alpha(\theta)$ is the function of the microplane spherical angle $\theta$ regarding to the bedding layers. Specifically, according to the experimental data for shales, the maximum strength occurs for the bedding planes either parallel or perpendicular to the loading direction while the minimum strength is typically associated with the sample orientation within the range 30 deg −60 deg. Thus, the phenomenon can be characterized by the proposed function (Fig. 6)

$$\alpha(\theta) = f_0\cos^2(2\theta) + 1 \tag{10}$$

where $f_0$ is a material parameter representing the degree of the strength variation, for example, for shales studied in this paper the parameter can be calibrated as 0.5.

(2) Normal compressive stress boundary

According to a series of experimental data on shales [1,6,7], it is obvious that the behavior of the shales is generally pressure sensitive essentially relating to the closure of microcracks. It is evident that the most significant closure effects occur in the orientation that the axial stress is normal to the bedding planes compared with other orientations. However, it is noteworthy that the closure effects also exist for $\theta =$ 90 deg corresponding to the axial stress parallel to the bedding planes due to the existence of initial cracks in shale matrix. Meanwhile, strain hardening due to the closure of internal micropores and microcracks is observed for all experimental investigations. Therefore, the normal compressive stress boundary is proposed to characterize the pressure sensitivity, the anisotropic microcracks closure effects as well as the hardening process with the following form:

$$\sigma_N^{b-} = \beta C_0\alpha(\theta) \tag{11}$$

where $C_0$ denotes the reference compressive strength, $\alpha(\theta)$ takes the same form in Eq. (10), $\beta$ the hardening parameter related to the confining pressure taking the form $\beta = a_1\sigma_c + a_2$ in which $\sigma_c$ is the confining pressure, and $a_1$, $a_2$ are the microplane material parameters related to the studied shales.

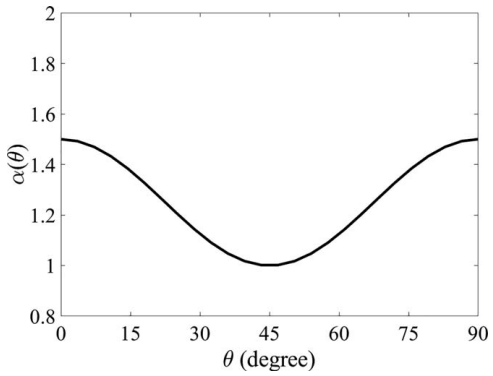


**Fig. 6 Schematic of the functions $\alpha(\theta)$ representing the anisotropic strength related to the bedding plane orientations**

(3) Shear stress boundary

Laboratory investigation shows that the nonlinear mechanical behavior such as the irreversible deformation, the confining pressure effects, and the frictional hardening is strongly related to the frictional sliding of microcracks under shear stress [15,27]. The shear strength generally increases with the confining pressure and varies with the angle from the bedding planes. It is apparent that the shear strength parallel to the bedding layers is minimal for low confining pressures; however, shear band often occurs in shale matrix under high confining pressures and fractures cross the bedding layers. Therefore, the description of the shear failure in the function of the orientation of bedding planes and confining pressures is given as

$$\sigma_T^b = \beta S_0\alpha(\theta) \tag{12}$$

where $S_0$ is the reference shear strength, $\alpha(\theta)$ is consistent with the definition in Eq. (10), and $\beta$ the hardening parameter associated with the confining pressure. As the shear elastic stress is pulled back to the stress boundary, the shear stress resultant force $\sigma_T = \sqrt{\sigma_M^2 + \sigma_L^2}$ is used as the criterion, and the final shear stress component value is obtained according to the vector direction of the respective components.

**3.2 The Damage Modeling.** As is known that the damage process is inevitable for most rock-like materials due to the initial and induced microcracks, and the orientation distribution of induced microcracks in most rock materials depends strongly on the loading path and leads to pronounced anisotropic behavior [28–30]. The high asymmetrical failures under the tensile and the compressive stress are strongly associated with the state of microcracks. The microcracks are generally open and propagate perpendicular to the loading direction under the tensile stress, but the frictional sliding along the crack surfaces mainly determines the mechanical behavior of closed microcracks under compression stress. Therefore, the induced anisotropic behavior related to the strong asymmetrical failure is required to be considered in the constitutive model. In the present work, two-scalar damage variables $d_t$ for the tensile damage and $d_s$ for the shear damage are introduced to describe the asymmetrical failure mechanisms.

The damage criterion should be derived in the framework of irreversible thermodynamics; however, for the sake of simplicity, an explicitly physical equation is adopted in the present work. Based on the physical phenomena in shales, the tensile damage is induced by the tensile strains with opening cracks, but the compressive damage is generally associated with the frictional sliding along the closed crack surfaces. Therefore, two damage evolution equations for the tensile and the shear stress conditions based on the previous works are proposed

$$d_t = 1 - e^{-b_1\langle\varepsilon_N^+ - \varepsilon_N^0\rangle}, \quad d_s = 1 - e^{-b_2\langle\varepsilon_T - \varepsilon_T^0 - \varepsilon_v\rangle} \tag{13}$$

where $\varepsilon_N^+$ is the microplane normal tensile normal strain, $\varepsilon_T$ the microplane shear strain, $\varepsilon_v$ the microplane volume strain, $b_1$, $b_2$ the material parameters that controls the rate of damage evolution, and $\varepsilon_N^0$, $\varepsilon_T^0$ the initiation threshold of the normal tensile damage and the shear damage, respectively.

According to the analysis of the induced damage related to the failure mechanisms, it is necessary to introduce the damage evolution equations to the normal tensile and shear boundaries, respectively. Therefore, in the framework of microplane theory, the final stress boundaries can be defined as

$$\begin{aligned}\sigma_N^{b+} &= (1 - d_t)T_0\alpha(\theta)\\ \sigma_N^{b-} &= \beta C_0\alpha(\theta)\\ \sigma_T^b &= (1 - d_s)\beta S_0\alpha(\theta)\end{aligned} \tag{14}$$

To this end, a damage constitutive model for the damage behavior of the highly anisotropic shales is fully established.

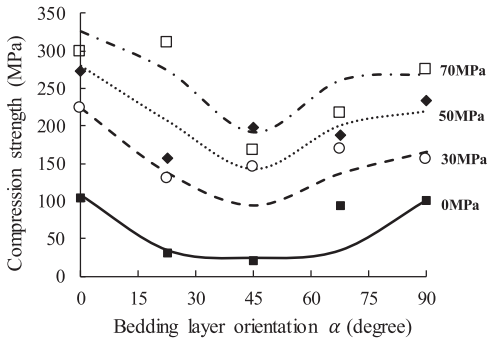


**Fig. 7 Comparison between experimental tests and the numerical simulation of compression strengths for different bedding layer orientations**

## 4 The Parameter Calibration and the Numerical Simulation

The proposed damage constitutive model is then implemented into a finite element commercial package ABAQUS by VUMAT material subroutine. In order to calibrate and validate the model, two types of shales are investigated according to the experimental data. As a medium degree of anisotropic rocks, the shale from West Hubei and East Chongqing in China (WHEC) is calibrated and studied. The proposed model is then applied to a strongly anisotropic shale from Tournemire in France to show the predictive ability for high degree of anisotropic shales.

**4.1 Application to the WHEC Shales.** The samples of the WHEC shale were taken from Shizhu, Chongqing belonging to the Lower Silurian Longmaxi formation. The shale in this area is widely distributed with large thickness and high organic matter, mainly composed of brittle minerals such as quartz and clay. Among them, the highest content of quartz is up to 51%, and the content of brittle minerals such as K-feldspar and albite up to 61.4%, which is very significant. The WHEC shales were conducted with scanning electron microscope (SEM) and triaxial compression tests for systematically investigating the microstructures, the physical and mechanical parameters such as the elastic modulus, the tensile strength, the compressive strength, and failure modes to reveal the anisotropic properties and failure mechanisms [31]. The elastic parameters of the experimental data are as follows:

$$E_{\perp}=14.21\ \text{GPa},\quad E_{/\!/}=22.9\ \text{GPa},\quad \nu_{\perp}=0.36,\quad \nu_{/\!/}=0.28,\quad G_{/\!/}=6.51\ \text{GPa} \tag{15}$$

For the parameters of the inelastic part, it is calibrated by the experimental uniaxial and the triaxial compressive strengths with different bedding layer orientations (Fig. 7). The tensile damage parameters are approximated by the Brazilian splitting strength parameters, and the compression damage parameters are calibrated by a set of experimental data, and the remaining data are reserved for the comparative analysis. All calibrated parameters are listed in Table 2. The remaining parameters $a_1$, $a_2$ are fixed parameters as follows:$a_1 = 0.05$/MPa, $a_2 = 1.0$, and the normal strain thresholds are taken as $\varepsilon_N^0 = 1.5\times10^{-4}$, $1.0\times10^{-4}$, $1.8\times10^{-4}$, and $1.2\times10^{-4}$.

Three angles between the core drilling direction and the bedding layers are investigated as 0 deg, 45 deg, and 90 deg (Fig. 8(*a*)). The angle between the loading direction (the uniform arrows along $z$-axis) and the bedding plane (dashed line) is shown in Fig. 8(*b*).

The proposed model is performed to simulate the WHEC shales for a series triaxial tests under different confining pressures and bedding layer orientations. The comparison between the numerical results and the experimental data points is shown in Fig. 9. It is noted that the numerical results are generally well agreed with the laboratory data. The model is capable of characterizing the main anisotropic characteristics such as the strength, the nonlinear mechanical behavior, and the effects of the confining pressure. It is also noted that the model can further describe the residual strength after peak strength, the increase of the peak and residual strength with the confining pressure related to the effects of the closure of microcracks. As expected that the strength of the shale for $\alpha = 45$ deg is obviously lower than the case for $\alpha = 0$ deg and $\alpha = 90$ deg which is consistent with the U-shaped distribution of the shale peak strength from the experimental investigations. The numerical simulation also exhibits that the WHEC shales are mainly characterized by elastic-brittle damage mechanical behavior which reveals the fact that the shale is mainly composed of brittle minerals. It is worth noting that comparing with the compression shear failure for $\alpha = 90$ deg, the failure mechanism for $\alpha = 0$ deg and $\alpha = 45$ deg is mainly splitting damage characterized by the tensile damage parameters due to the existence of bedding layers.

**Table 2 Inelastic material parameters for WHEC shales under triaxial compression tests**

| | Mode I | Mode II | Mode III | Mode IV |
|---|---|---|---|---|
| $T_0$/MPa | 18 | 0.1 | 7 | 3 |
| $C_0$/MPa | 55 | 50 | 36 | 5 |
| $S_0$/MPa | 28 | 20 | 31 | 5.5 |
| $\varepsilon_T^0$ | 0.012 | 0.01 | 0.0025 | 0.01 |
| $b_1$ | 600 | 200 | 800 | 100 |
| $b_2$ | 200 | 2000 | 1000 | 200 |

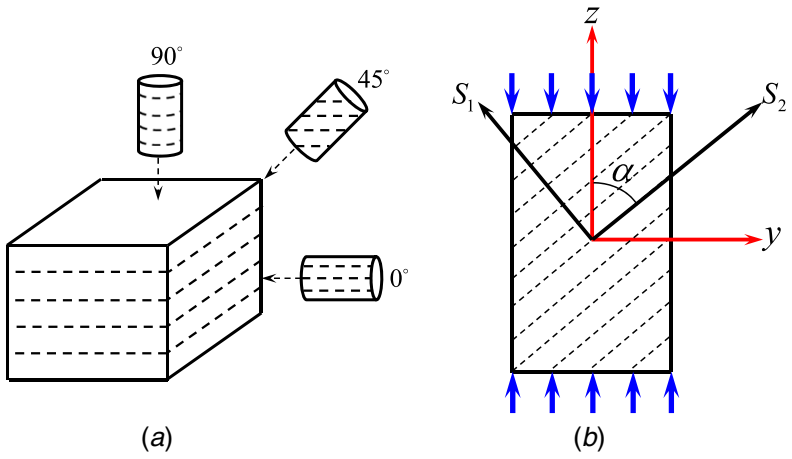


**Fig. 8 Illustration of specimens with different bedding layer orientations**

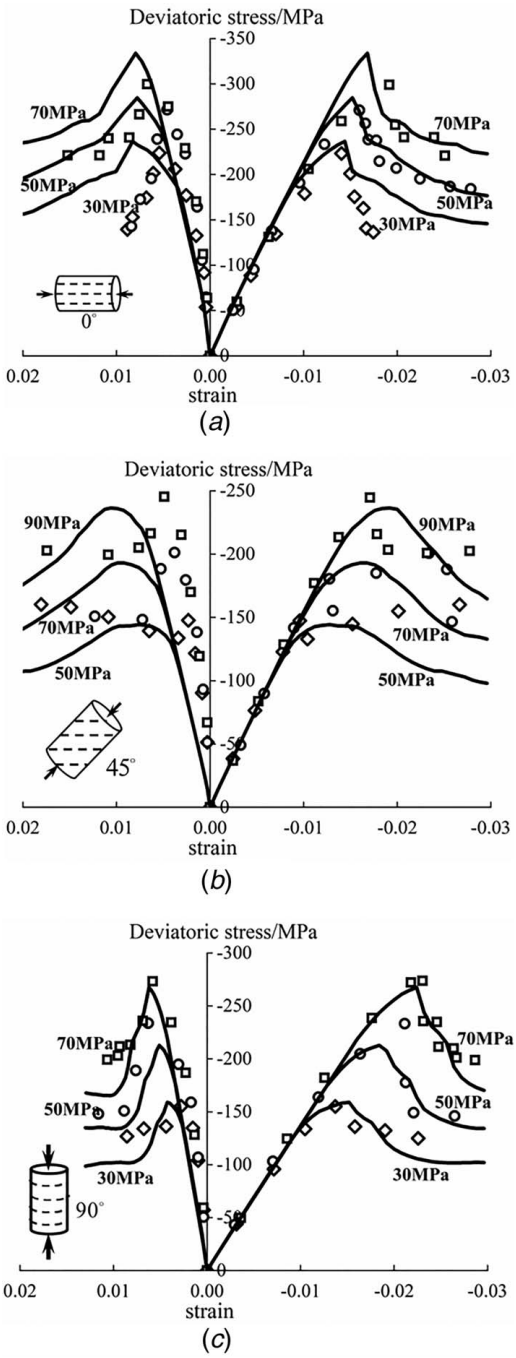


**Fig. 9 Numerical results of the triaxial tests under different confining pressures and different bedding plane orientations: (*a*) $\alpha = 0$ deg, (*b*) $\alpha = 45$ deg, and (c) $\alpha = 90$ deg**

Those parameters are approximately calibrated by the rough estimation of the tensile strength provided by the Brazilian split-cylinder test, especially for the anisotropic shale with rather scattered results. Thus, the results for $\alpha = 90$ deg have a better match with the experimental data when compared with the other two cases. In general, the proposed spectral damage microplane model is capable of predicting the macroscopic anisotropic mechanical behavior of anisotropic shales. However, further validation of the predictive ability for highly anisotropic shales is still needed.

**4.2 Application to the Tournemire Shales.** A strongly anisotropic shale from Tournemire in France is then studied. The Tournemire shale is taken from the large Toarcian shale area in the Tournemire region of the Central Plateau in France. The mineral composition includes kaolinite (27.5%), illite (16.5%), quartz (19%), calcite (15%), and other minerals (22%). The typical anisotropic behavior of Tournemire shale was studied and its failure modes were divided into the shear failure and the tensile failure [7]. It is pointed out that the elastic properties of shales are affected by confining pressure, and the nonlinear elastic constitutive relationship should be used. Since the core of this study is to simulate the nonlinear anisotropic behavior of shales, the elastic parameter is referred as follows [12]:

$$E_{\perp}=7000\ \text{MPa},\quad E_{/\!/}=22000\ \text{MPa},\quad \nu_{\perp}=0.12,\quad \nu_{/\!/}=0.14,\quad G_{/\!/}=4000\ \text{MPa} \tag{16}$$

For the inelastic parameters, it is first calibrated by the compressive strength under different confining pressures with different bedding plane orientations as shown in Fig. 10. The tensile damage parameters are calibrated approximately by the Brazilian splitting strength parameters. The compression damage parameters are calibrated using a set of experimental data, and the remaining experimental data are reserved for comparative analysis. All calibrated parameters in the model are listed in Table 3 and the normal strain thresholds are $\varepsilon_N^0 = 1.8\times10^{-2}$, $1.5\times10^{-5}$, $1.2\times10^{-5}$, and $1.4\times10^{-4}$.

Different from the WHEC shale, the Tournemire shale possesses strongly anisotropic properties, namely, the elastic moduli ratio between the anisotropic and transverse direction (degree of anisotropy) is high to be 3.14. Meanwhile, the Tournemire shale exhibits an elastic-brittle damage behavior under low confining pressure, but as the confinement grows the pronounced prepeak hardening process is observed with the rapid postpeak softening and the residual strength. The proposed model is applied to simulate Tournemire shales for a series triaxial tests under different confining pressures and different bedding layer orientations and the comparison is shown in Fig. 11. In general, the numerical results are well fitted with the main mechanical behavior of the highly anisotropic shales. The comparison shows that the model can well describe the gradual prepeak hardening, the plastic deformation, and the gradual weakening of the brittle feature as well as the progressive increase of the ductile feature under the growth of the confining pressure. It also reveals that the strength at $\alpha = 45$ deg is significantly lower than the ones at $\alpha = 0$ deg and 90 deg. It is noted that the numerical simulation of the postpeak softening behavior under low confinement is not quite satisfactory, but in general the proposed spectral damage microplane model can be used to predict the anisotropic behavior of highly anisotropic shales.

## 5 Concluding Remarks

(1) A spectral microplane damage model is developed for the anisotropic damage behavior of the transversely isotropic

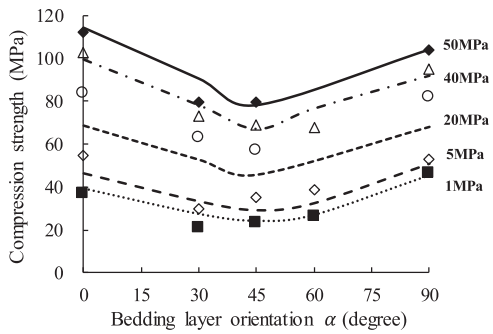


**Fig. 10 Comparison between experimental tests and numerical simulation of compression strength for different bedding layer orientations**

**Table 3 Inelastic material parameters for Tournemire shales under triaxial compression tests**

| | Mode I | Mode II | Mode III | Mode IV |
|---|---|---|---|---|
| $T_0$/MPa | 5 | 10 | 12 | 1 |
| $C_0$/MPa | 30 | 50 | 28 | 1 |
| $S_0$/MPa | 5 | 12 | 14 | 7 |
| $\varepsilon_T^0$ | 0.0095 | 0.01 | 0.0065 | 0.019 |
| $b_1$ | 1500 | 200 | 2000 | 2000 |
| $b_2$ | 300 | 1000 | 1100 | 500 |

shales. The modeling challenge of high degree of anisotropic shales is theoretically solved without limitation on the degree of anisotropy compared with other microplane models.

(2) The elastic stiffness tensor of anisotropic shales is decomposed into four eigenmodes corresponding to different loading path with negligible interactions. This feature allows to define constitutive laws from microscopic level to consider the physical mechanisms such as the effects of the mesostructure, the damage induced by the splitting and sliding process related to the bedding layers.

(3) A two-scalar damage model is proposed to characterize the tensile and shear damage related to the opening and closure of microcracks under different stress conditions. The induced anisotropic postpeak softening depending on the loading path and the effects of microcracks are thus well described.

(4) Comparison between the numerical simulation and the experimental data shows a good agreement for both weakly and highly anisotropic shales. The proposed model generally provides satisfactory predictions including the prepeak nonlinear behavior, the failure strength, and the postpeak softening under different confining pressures and different bedding plane orientations.

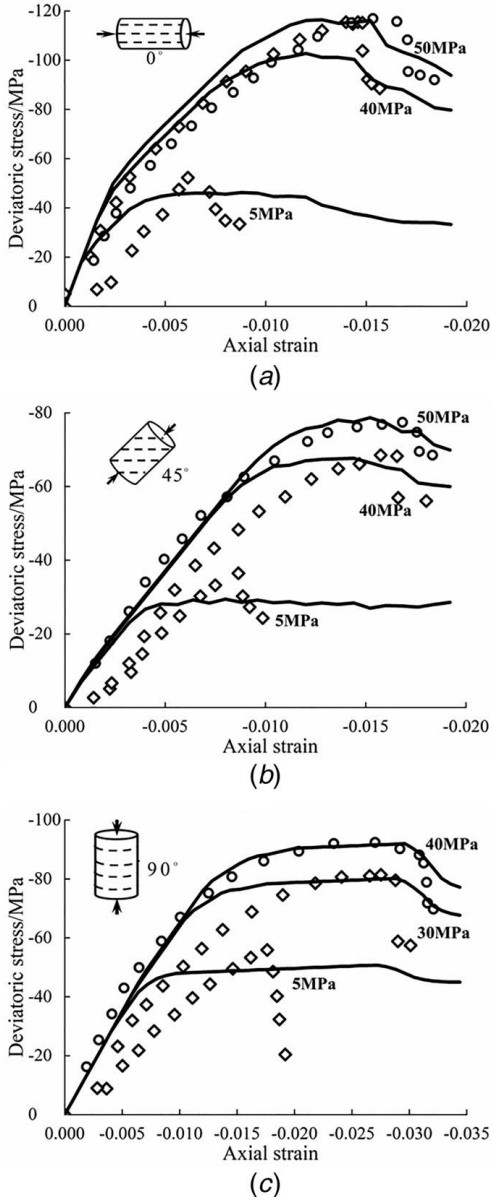


**Fig. 11 Comparison between experimental tests and numerical simulation of triaxial tests under different confining pressures and different bedding plane orientations: (*a*) $\alpha = 0$ deg, (*b*) $\alpha = 45$ deg, and (c) $\alpha = 90$ deg**

## Acknowledgment

The authors gratefully acknowledge the support from the National Natural Science Foundation of China (grant Nos. 11772331, 11572323, 11802332, and 11572344), Beijing Municipal Natural Science Foundation (No. 2202066), Key Research Program of Frontier Sciences of the Chinese Academy of Sciences (ZDBS-LY-JSC014), Chinese Academy of Sciences via the "Hundred Talent Program," Strategic Priority Research Program of the Chinese Academy of Sciences (No. XDB22040501), and the State Key Laboratory of Structural Analysis for Industrial Equipment, Dalian University of Technology (No. GZ19102).

## Appendix A

The stress matrix ($\boldsymbol{\sigma}$) and the strain matrix ($\boldsymbol{\varepsilon}$) in the elastic stress–strain relation of anisotropic material $(\boldsymbol{\sigma}) = [\boldsymbol{C}](\boldsymbol{\varepsilon})$ takes the form of six-dimensional vector in terms of components as

$$(\boldsymbol{\sigma}) = \begin{pmatrix} \sigma_{11} & \sigma_{22} & \sigma_{33} & \sqrt{2}\sigma_{23} & \sqrt{2}\sigma_{13} & \sqrt{2}\sigma_{12} \end{pmatrix}^T \tag{A1}$$

$$(\boldsymbol{\varepsilon}) = \begin{pmatrix} \varepsilon_{11} & \varepsilon_{22} & \varepsilon_{33} & \sqrt{2}\varepsilon_{23} & \sqrt{2}\varepsilon_{13} & \sqrt{2}\varepsilon_{12} \end{pmatrix}^T \tag{A2}$$

where $[\boldsymbol{C}]$ is the $6 \times 6$ dimensional elastic stiffness matrix. With the eigenmatrix $[\boldsymbol{C}_I]$, the stress matrix ($\boldsymbol{\sigma}$) and the strain matrix ($\boldsymbol{\varepsilon}$) can be thus decomposed into orthogonal eigenstresses ($\boldsymbol{\sigma}_I$) and eigenstrains ($\boldsymbol{\varepsilon}_I$)

$$(\boldsymbol{\sigma}_I) = [\boldsymbol{C}_I](\boldsymbol{\sigma}),\ (\boldsymbol{\varepsilon}_I) = [\boldsymbol{C}_I](\boldsymbol{\varepsilon}) \tag{A3}$$

Coupling with the former formulation and some deduction, it can be easily proven that $(\boldsymbol{\sigma}) = \sum_I (\boldsymbol{\sigma}_I)$, $(\boldsymbol{\varepsilon}) = \sum_I (\boldsymbol{\varepsilon}_I)$, and the relation between the eigenstress and the eigenstrain can be thus formulated as

$$(\boldsymbol{\sigma}_I) = \lambda_I(\boldsymbol{\varepsilon}_I) \tag{A4}$$

In the microplane model, the macroscopic strain ($\boldsymbol{\varepsilon}$) can be projected to be the microplane strain vectors ($\boldsymbol{\varepsilon}_P$)

$$(\boldsymbol{\varepsilon}_P) = [P](\boldsymbol{\varepsilon}) \tag{A5}$$

where $(\boldsymbol{\varepsilon}_P) = (\varepsilon_N, \varepsilon_L, \varepsilon_M)^T$ and $\varepsilon_N$, $\varepsilon_M$, $\varepsilon_L$ denote the normal and the two tangent components. $[P]$ is the projection matrix

$$[P] = \begin{bmatrix} N_{11} & N_{22} & N_{33} & \sqrt{2}N_{23} & \sqrt{2}N_{13} & \sqrt{2}N_{12} \\ M_{11} & M_{22} & M_{33} & \sqrt{2}M_{23} & \sqrt{2}M_{13} & \sqrt{2}M_{12} \\ L_{11} & L_{22} & L_{33} & \sqrt{2}L_{23} & \sqrt{2}L_{13} & \sqrt{2}L_{12} \end{bmatrix} \tag{A6}$$

where $N_{ij} = n_i n_j$, $M_{ij} = (m_i n_j + m_j n_i)/2$, $L_{ij} = (l_i n_j + l_j n_i)/2$, in which $n_i$ is the unit normal vector and $m_i$, $l_i$ are the two orthogonal unit vectors of the microplane in the global coordinate system with

local Cartesian coordinates $\boldsymbol{l} = m \times \boldsymbol{n}$. Similarly, the microplane strain ($\boldsymbol{\varepsilon}_P$) can be also decomposed with the spectral theorem as

$$(\boldsymbol{\varepsilon}_{PI}) = [P_I](\boldsymbol{\varepsilon}) \tag{A7}$$

where $[P_I] = [P][\boldsymbol{C}_I]$ and $(\boldsymbol{\varepsilon}_P) = \sum_I (\boldsymbol{\varepsilon}_{PI})$.

## Appendix B

For the convenience of the calculation, the local stress can be transferred as

$$(\boldsymbol{\sigma}') = [\boldsymbol{T}_\sigma](\boldsymbol{\sigma}) \tag{B1}$$

where the rotated and the original stress are $(\boldsymbol{\sigma}') = (\sigma'_1, \sigma'_2, \sigma'_3, \sigma'_4, \sigma'_5, \sigma'_6)^T$ and $(\boldsymbol{\sigma}) = (\sigma_1, \sigma_2, \sigma_3, \sigma_4, \sigma_5, \sigma_6)^T$. The rotational matrix $[\boldsymbol{T}_\sigma]$ can be expressed as

$$[\boldsymbol{T}_\sigma] = \begin{bmatrix} \cos^2\alpha & \sin^2\alpha & 0 & 2\cos\alpha\sin\alpha & 0 & 0 \\ \sin^2\alpha & \cos^2\alpha & 0 & -2\cos\alpha\sin\alpha & 0 & 0 \\ 0 & 0 & 1 & 0 & 0 & 0 \\ -\cos\alpha\sin\alpha & \cos\alpha\sin\alpha & 0 & \cos^2\alpha - \sin^2\alpha & 0 & 0 \\ 0 & 0 & 0 & 0 & \cos\alpha & -\sin\alpha \\ 0 & 0 & 0 & 0 & \sin\alpha & \cos\alpha \end{bmatrix} \tag{B2}$$

The local strain can be transferred by the rotation matrix as well and takes the form

$$(\boldsymbol{\varepsilon}') = [\boldsymbol{T}_\varepsilon](\boldsymbol{\varepsilon}) \tag{B3}$$

## Appendix C

According to the spectral decomposition theorem, the elastic stiffness matrix $[\boldsymbol{C}]$ can be decomposed into four independent analytical eigenvalues

$$(\lambda_I)^{-1} = \frac{1+\nu_{/\!/}}{E_{/\!/}} \tag{C1}$$

$$(\lambda_{II})^{-1} = \frac{1-\nu_{/\!/}}{2E_{/\!/}} + \frac{1}{2E_\perp} - \sqrt{\left(\frac{1-\nu_{/\!/}}{2E_{/\!/}} - \frac{1}{2E_\perp}\right)^2 + 2\left(\frac{\nu_\perp}{E_{/\!/}}\right)^2} \tag{C2}$$

$$(\lambda_{III})^{-1} = \frac{1-\nu_{/\!/}}{2E_{/\!/}} + \frac{1}{2E_\perp} + \sqrt{\left(\frac{1-\nu_{/\!/}}{2E_{/\!/}} - \frac{1}{2E_\perp}\right)^2 + 2\left(\frac{\nu_\perp}{E_{/\!/}}\right)^2} \tag{C3}$$

$$(\lambda_{IV})^{-1} = \frac{1}{2G_\perp} \tag{C4}$$

with the corresponding eigenmatrices

$$[\boldsymbol{C}_I] = \begin{bmatrix} 0.5 & -0.5 & 0 & 0 & 0 & 0 \\ -0.5 & 0.5 & 0 & 0 & 0 & 0 \\ 0 & 0 & 0 & 0 & 0 & 0 \\ 0 & 0 & 0 & 0 & 0 & 0 \\ 0 & 0 & 0 & 0 & 0 & 0 \\ 0 & 0 & 0 & 0 & 0 & 1 \end{bmatrix} \tag{C5}$$

$$[\boldsymbol{C}_{II}] = \begin{bmatrix} \cos^2\omega/2 & \cos^2\omega/2 & \cos\omega\sin\omega/\sqrt{2} & 0 & 0 & 0 \\ \cos^2\omega/2 & \cos^2\omega/2 & \cos\omega\sin\omega/\sqrt{2} & 0 & 0 & 0 \\ \cos\omega\sin\omega/\sqrt{2} & \cos\omega\sin\omega/\sqrt{2} & \sin^2\omega & 0 & 0 & 0 \\ 0 & 0 & 0 & 0 & 0 & 0 \\ 0 & 0 & 0 & 0 & 0 & 0 \\ 0 & 0 & 0 & 0 & 0 & 0 \end{bmatrix} \tag{C6}$$

$$[\boldsymbol{C}_{III}] = \begin{bmatrix} \sin^2\omega/2 & \sin^2\omega/2 & -\cos\omega\sin\omega/\sqrt{2} & 0 & 0 & 0 \\ \sin^2\omega/2 & \sin^2\omega/2 & -\cos\omega\sin\omega/\sqrt{2} & 0 & 0 & 0 \\ -\cos\omega\sin\omega/\sqrt{2} & -\cos\omega\sin\omega/\sqrt{2} & \cos^2\omega & 0 & 0 & 0 \\ 0 & 0 & 0 & 0 & 0 & 0 \\ 0 & 0 & 0 & 0 & 0 & 0 \\ 0 & 0 & 0 & 0 & 0 & 0 \end{bmatrix} \tag{C7}$$

$$[\boldsymbol{C}_{IV}] = \begin{bmatrix} 0 & 0 & 0 & 0 & 0 & 0 \\ 0 & 0 & 0 & 0 & 0 & 0 \\ 0 & 0 & 0 & 0 & 0 & 0 \\ 0 & 0 & 0 & 1 & 0 & 0 \\ 0 & 0 & 0 & 0 & 1 & 0 \\ 0 & 0 & 0 & 0 & 0 & 0 \end{bmatrix} \tag{C8}$$

where $\omega$ is the eigen angle defined by the independent elastic parameters as

$$\tan\ 2\omega = \frac{-2\sqrt{2}\nu_{\perp}/E_{\perp}}{(1-\nu_{/\!/})/E_{/\!/} - 1/E_{\perp}} \tag{C9}$$

and this parameter can be treated as an overall indicator for material anisotropy.

## References


[1] McLamore, R., and Gray, K. E., 1967, "The Mechanical Behavior of Anisotropic Sedimentary Rocks," J. Eng. Ind., **89**(1), pp. 62–73.
[2] Amadei, B., 1996, "Importance of Anisotropy When Estimating and Measuring In Situ Stresses in Rock," Int. J. Rock Mech. Min. Sci. Geomech. Abstr., **33**(3), pp. 293–325.
[3] Lonardelli, I., Wenk, H. R., and Ren, Y., 2007, "Preferred Orientation and Elastic Anisotropy in Shales," Geophysics., **72**(2), pp. D33–D40.
[4] Sondergeld, C. H., and Rai, C. S., 2011, "Elastic Anisotropy of Shales," Leading Edge, **30**(3), pp. 324–331.
[5] Lisjak, A., Grasselli, G., and Vietor, T., 2014, "Continuum–Discontinuum Analysis of Failure Mechanisms Around Unsupported Circular Excavations in Anisotropic Clay Shales," Int. J. Rock Mech. Min. Sci., **65**, pp. 96–115.
[6] Kwasniewsi, M. A., 1993, "Mechanical Behaviour of Anisotropic Rocks," *Comprehensive Rock Engineering*, J. Hudson, ed., Vol. I: Fundamentals, Pergamon Press, Oxford.
[7] Niandou, H., Shao, J. F., Henry, J. P., and Fourmaintraux, D., 1997, "Laboratory Investigation of the Mechanical Behaviour of Tournemire Shale," Int. J. Rock Mech. Min. Sci., **34**(1), pp. 3–16.
[8] Sone, H., and Zoback, M. D., 2013, "Mechanical Properties of Shale-Gas Reservoir Rocks—Part 1: Static and Dynamic Elastic Properties and Anisotropy," Geophysics, **78**(5), pp. D378–D389.
[9] Heller, R., Vermylen, J., and Zoback, M., 2014, "Experimental Investigation of Matrix Permeability of Gas Shales," AAPG Bull., **98**(5), pp. 975–995.
[10] Estrada, J. M., and Bhamidimarri, R., 2016, "A Review of the Issues and Treatment Options for Wastewater From Shale Gas Extraction by Hydraulic Fracturing," Fuel, **182**, pp. 292–303.
[11] Duveau, G., Shao, J. F., and Henry, J. P., 1998, "Assessment of Some Failure Criteria for Strongly Anisotropic Geomaterials," Mech. Cohes.-Frict. Mater., **3**(1), pp. 1–26.
[12] Pietruszczak, S., Lydzba, D., and Shao, J. F., 2002, "Modelling of Inherent Anisotropy in Sedimentary Rocks," Int. J. Solids Struct., **39**(3), pp. 637–648.
[13] Hoek, E., and Brown, E. T., 1980, "Empirical Strength Criterion for Rock Masses," J. Geotech. Eng. Div., **106**(9), pp. 1013–1035.
[14] Duveau, G., and Shao, J. F., 1998, "A Modified Single Plane of Weakness Theory for the Failure of Highly Stratified Rocks," Int. J. Rock Mech. Min. Sci., **35**(6), pp. 807–813.
[15] Jaeger, J. C., 1960, "Shear Failure of Anistropic Rocks," Geol. Mag., **97**(1), pp. 65–72.
[16] Zhu, Q., Kondo, D., Shao, J., and Pensee, V., "Micromechanical Modelling of Anisotropic Damage in Brittle Rocks and Application," Int. J. Rock Mech. Min. Sci., **45**(4), pp. 467–477.
[17] Pensée, V., Kondo, D., and Dormieux, L., 2002, "Micromechanical Analysis of Anisotropic Damage in Brittle Materials," J. Eng. Mech., **128**(8), pp. 889–897.
[18] Taylor, G. I., 1938, "Plastic Strain in Metals," J. Inst. Met., **62**, pp. 307–324.
[19] Bazant, Z. P., 1984, "Microplane Model for Strain-Controlled Inelastic Behaviour," *Mechanics of Engineering Materials*, C. S. Desai, and R. H. Gallagher, eds., Wiley, London, Chapter 3.
[20] Bažant, Z. P., and Planas, J., 1998, "Fracture and Size Effect in Concrete and Other Quasibrittle Materials," *New Directions in Civil Engineering*, W. F. Chen, ed., CRC Press, London.
[21] Bazant, Z. P., and Kim, J.-K., 1986, "Creep of Anisotropic Clay: Microplane Model," J. Geotech. Eng., **112**(4), pp. 458–475.
[22] Brocca, M., Bažant, Z. P., and Daniel, I. M., 2001, "Microplane Model for Stiff Foams and Finite Element Analysis of Sandwich Failure by Core Indentation," Int. J. Solids Struct., **38**(44), pp. 8111–8132.
[23] Li, C., Caner, F. C., Chau, V. T., and Bažant, Z. P., 2017, "Spherocylindrical Microplane Constitutive Model for Shale and Other Anisotropic Rocks," J. Mech. Phys. Solids, **103**, pp. 155–178.
[24] Cusatis, G., Beghini, A., and Bažant, Z. P., 2008, "Spectral Stiffness Microplane Model for Quasibrittle Composite Laminates-Part I: Theory," J. Appl. Mech., **75**(2), p. 021009.
[25] Bazant, Z. P., Xiang, Y. Y., and Prat, P. C., 1996, "Microplane Model for Concrete. I. Stress-Strain Boundaries and Finite Strain," J. Eng. Mech., **122**(3), pp. 245–254.
[26] Lee, Y.-K., and Pietruszczak, S., 2015, "Tensile Failure Criterion for Transversely Isotropic Rocks," Int. J. Rock Mech. Min. Sci., **79**, pp. 205–215.
[27] Platt, J. P., and Vissers, R. L. M., 1980, "Extensional Structures in Anisotropic Rocks," J. Struct. Geol., **2**(4), pp. 397–410.
[28] Mazars, J., 1986, "A Description of Micro- and Macroscale Damage of Concrete Structures," Eng. Fract. Mech., **25**(5), pp. 729–737.
[29] Lemaitre, J., 1996, *A Course on Damage Mechanics*, Springer-Verlag, Berlin Heidelberg.
[30] Voyiadjis, G. Z., Taqieddin, Z. N., and Kattan, P. I., 2008, "Anisotropic Damage–Plasticity Model for Concrete," Int. J. Plast., **24**(10), pp. 1946–1965.
[31] Zhang, Y. Z., 2016, "Study on Anisotropy of Mechanical Properties of the Shale in West Hubei and East Chongqing (in Chinese)," Southwest University of Science and Technology, Sichuan, China.